

RESEARCH ARTICLE

Numerical Analysis on The Effects of Stagger, Thickness, and Curvature on The Propulsion of Tandem Airfoil

Andrew G. Zebua¹, Sheila Tobing^{2,3*}, Tajuddin Nur⁴, and Mohammad Akita Indianto^{2,3}

¹Department of Mechanical Engineering, Atma Jaya Catholic University of Indonesia, 15345 Jakarta, Indonesia

²Energy System Engineering Graduate Program, Faculty of Engineering, University of Indonesia, 16425 Depok, Indonesia

³Tropical Renewable Energy Center, Faculty of Engineering, University of Indonesia, 16425 Depok, Indonesia

⁴Department of Electrical Engineering, Atma Jaya Catholic University of Indonesia, 15345 Jakarta, Indonesia

ABSTRACT - The study of the aerodynamics of flapping airfoils is crucial to understand the flight of natural flyers and its potential applications in developing micro air vehicles and wind/water turbine blades. There has been much research on the aerodynamics of flapping wings recently, but there is only a little research relating to the tandem airfoil. Therefore, this study is conducted to determine the aerodynamic characteristics of the tandem airfoil at $Re = 100000$, typical of insect flight. The tandem airfoil is plunging and pitching harmonically. This study numerically analyzes the effects of stagger, thickness, and curvature on tandem airfoil propulsion. The effects of stagger are studied using NACA 0012, while the effects of thickness are analyzed on NACA 0012, 0015, 0020 and 0030. The simulations to study the effects of curvature are conducted using NACA 0030. The optimum distance of the stagger is $X/c = 2.5$, but the propulsive efficiency of tandem NACA 0012 is still smaller than two single NACA 0012 airfoils. For the most optimum thickness at 30% of the chord length, the propulsive efficiency of tandem NACA 0030 is higher than two single NACA 0030 airfoils. Meanwhile, the most optimum curvature is 0% because the increase in curvature of the airfoil reduces propulsive efficiency.

ARTICLE HISTORY

Received : 19th Nov 2022
 Revised : 20th June 2023
 Accepted : 30th June 2023
 Published : 21st July 2023

KEYWORDS

Flapping airfoil;
Micro air vehicles;
Tandem airfoil;
Stagger

1.0 INTRODUCTION

Research on the aerodynamics of flapping airfoils is significant for understanding the nature of natural flight and developing micro air vehicles. Micro air vehicles are crewless aircraft with a maximum dimension of 15 cm that operates at a speed of 10 m/s-20 m/s [1]. Many studies on flapping wing MAVs, which are inspired by natural flyers like insects and birds, have been conducted by many researchers. Several notable recent studies are by Djojodihardjo and Ramli [2], Bie and Lie [3], Liu et al. [4], Wang et al. [5], Olejnik et al. [6] and Joda, Mohmmmed and Tolouei [7]. Some of these studies focus on the aerodynamics and propulsion of flapping wing MAVs both numerically [3], [7], experimentally [6] and a combination of them [5]. The other studies focus on the flapping mechanism/kinematics [2], [4]. Despite the many advances in the design and development of MAVs, more study on the aerodynamics and propulsion of flapping airfoils/wings is needed.

In the last few decades, research on flapping airfoils has been carried out to study the flapping frequency, plunging amplitude, and phase difference between plunging and pitching. Koochesfahani [8] studied the wake flow pattern of an oscillating airfoil, while Tuncer and Platzer [9] studied the flow characteristics and wake profiles behind a flapping airfoil. Jones et al. [10] studied the reduced frequency and Strouhal number in NACA 0012. In contrast, Reuster et al. [11] studied the characteristics of NACA 0012 airfoil under dynamic-stall conditions from plunging and pitching motions. Lee et al. [12] studied the aerodynamic characteristics of unsteady-force-generation of insect flapping motion.

In addition to being carried out in numerical simulations, other research was also carried out experimentally. For example, Rival et al. [13] studied the characteristics of SD7003 airfoils under dynamic-stall conditions of plunging and pitching motion. Wu et al. [14] examined the wing structure of micro air vehicles for their optimum flight. Ren et al. [15] investigated the formation of irregular wake on oscillating NACA 0012. Mulder and Hoeijmakers [16] investigated the effects of Strouhal number and pitching amplitude on flapping wing propulsion. Brentjes and Hoeijmakers [17] studied the wake phenomenon in robotic bird flapping wings. Several studies were also conducted to study the effects of airfoil shape on the resulting propulsion. For example, Ashraf et al. [18] investigated the effects of the Reynolds number, thickness, and airfoil curvature on propulsion. Similar studies were also carried out by Yu et al. [19] regarding the effects of airfoil thickness, reduced frequency, Strouhal number, and Reynolds number. Research on the effects of shape was also conducted through experiments. For instance, Null et al. [20] studied the aerodynamic effects of curvature on the adaptive wing, while Dongli et al. [21] investigated the aerodynamic characteristics of different airfoil thicknesses. In addition to research on a single airfoil, there was research on the tandem airfoil conducted by Tuncer [22], who found that the tandem airfoil's propulsive efficiency increased by 40% compared to the single airfoil.

Previous studies on tandem airfoils usually focus on a single parameter. Broering [23] numerically studied the differential phase between the front wing and the rear wing, and later [24] examined the distance/stagger between the tandem airfoil at $Re = 5000$. Similar computational research on the phase difference and distance between the airfoils was conducted by Lim [25], but the airfoil model used was S1020 and at $Re = 1000$. Experiments were conducted by Zhang et al. [26]. They studied the aerodynamic characteristics of the flapping wing in the tandem configuration by giving a phase difference between the front wing and the rear wing. Seet et al. [27] studied the aerodynamic characteristics of NACA 4421 by providing a differential phase and distance between the front airfoil and rear airfoil.

Research conducted by Tuncer [16] found that the best stagger is at the distance of $X/c = 2$, but this contrasts with the research conducted by Broering [24], who showed that the resultant force and propulsive efficiency of the tandem wings remained constant for all wing spacings. Ashraf et al. [18] found that the best airfoil thickness was 20% of the chord length, which contrasts with Yu et al. [19], who argued that the best airfoil thickness was 12%.

More recent studies on tandem airfoil or wings are very diverse. Hsiang Lai [28] studied the effects of hindwing kinematics on the propulsive efficiency of a damselfly at $Re = 1060$. This study found that the optimal hindwing kinematics increased the thrust efficiency up to 22% compared with the original motion of the hindwing [28]. Hosseini [29] investigated numerically tandem Selig-Donovan 7003 (SD7003) airfoils at $Re = 30,000$ and found that the total lift-to-drag ratio for the optimum tandem configuration improved by up to 6.5% compared to two separated airfoils. There was also a numerical study by Chen [30]. Tandem elliptical airfoils undergoing pitching-plunging motions at $Re = 5000$ and the parameters varied were the angle-of-attack, phase difference and airfoil spacing [30]. The findings of this study were the tandem airfoils generated a higher lift and drag compared to isolated airfoils and that the optimal spacing between airfoils is from $1.5c$ to $2c$. The same elliptical airfoils and $Re = 5000$ but undergoing time-asymmetric flapping and various phase angles were studied by Wang et al. [31]. Bie [3] also studied tandem NACA 0012 airfoils at $Re = 34,410$ that underwent pitch and plunge motions. At a polar angle of -40° and a polar distance of $2c$, an increase in the lift coefficient by 78.1% was observed. However, at another setting of 30° and $1.5c$, a 51.6% decrease in the lift coefficient and a 13.1% decrease in the thrust coefficient were found. Despite the diversity in the airfoil types, the flapping kinematics and the airfoil/wing spacings, recent publications on tandem airfoils are work in the Reynolds number regime of the order of 10^3 and 10^4 .

Although there has been much research on the flapping airfoil, only a little investigation of the airfoil was carried out at $Re = 100,000$ regarding the effects of the tandem airfoil's stagger and the airfoil shape on propulsive efficiency. This Reynolds number range is typical for many applications of flapping kinematics, such as on micro air vehicles [32] and flapping/oscillating water/wind turbines [33]–[35]. The wide application of flapping kinematics makes it necessary to study the flow phenomena in this particular fluid regime thoroughly. Therefore, this paper focuses on determining the aerodynamic characteristics and propulsive efficiency of variations in tandem airfoil distances using NACA 0012, as well as the modification of the airfoil shape based on variations in thickness and curvature of the airfoil at $Re = 100,000$. The force of the tandem airfoils was compared with that of the summation of two isolated single airfoils to identify the effects of tandem configuration. Computational Fluid Dynamics (CFD), which has been established as a reliable method for studying aerodynamic phenomena [36]–[38], is used in this study.

2.0 COMPUTATIONAL SETUP AND VALIDATION

2.1 Computational Setup

As the first step in conducting the present research, the author uses a validation case based on the numerical simulations of Tuncer and Platzer [16]. The simulation is conducted in this study using ANSYS FLUENT 17.2 program. The flow is modeled using the turbulence model of $k-\omega$ SST. The domain used in this simulation is shown in Figure 1. The grid consists of 2 types: the structured grid for the domain inside the circle and the unstructured grid for the domain outside the circle.

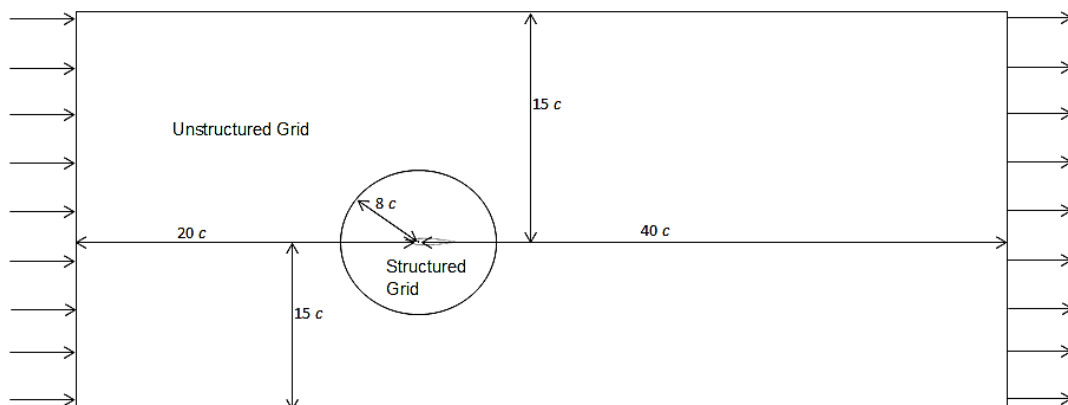


Figure 1. Domain design

2.2 Grid and Time Step Independence Study

The validation process is done with Tuncer and Platzler's [22] publication as a reference. Plunging a single NACA 0012 airfoil is used at Reynold numbers 3×10^6 to find how many grids and time-step produce the closest drag coefficient values compared to the reference. Values of reduced frequencies used are 0.3, 0.5, and 1. The independent grid and time-step study are conducted with three grids and three time-steps per flapping cycle to verify the numerical setup. The coarse grid has 223870 elements, the medium grid 479040 elements, and the fine grid 1000670 elements. The independent grid study is conducted using 200-time steps per flapping cycle. This study shows that the error of the 479070 grid is the smallest and thus, it is used in further simulations (as shown in Table 1).

The independent time-step study uses the medium grid with three variations, 200, 400, and 800-time steps per flapping cycle. A summary of the independent studies is shown in Table 1 and Table 2. Based on these results, it is found that the medium grid with 200-time steps merely shows a maximum error of 3.68%, and there is an insignificant difference between the results of 200, 400, and 800-time steps. Therefore, the medium grid with 200 time-steps per cycle is used in the subsequent simulations.

Table 1. The time-averaged drag coefficient for grid independence

k	$C_{T_{mean}}$ [22]	223870 elements	479070 elements	1000670 elements	Medium grid error (%)
0.3	0.0163	0.0158	0.0157	0.0152	3.68
0.5	0.0477	0.0486	0.0485	0.0485	1.67
1	0.1703	0.1690	0.1700	0.1700	0.17

Table 2. The time-averaged drag coefficient for time-step independence

k	$C_{T_{mean}}$ [22]	200 time-step	400 time-step	800 time-step	Error (%)
0.3	0.0163	0.0157	0.0157	0.0157	3.68
0.5	0.0477	0.0485	0.0485	0.0485	1.67
1	0.1703	0.1700	0.1690	0.1690	0.17

2.3 Flapping Kinematics

The sinusoidal plunging motion is determined using this equation $h(t) = h \sin(2\pi ft)$ with the following values of $h = 0.5$ m, $k = 2$ ($St = 0.31$) and $f = 0.4648$ Hz, with h is the dimensional plunging amplitude (m), f is the plunging and pitching frequency (Hz), $k = \frac{2\pi fc}{U_{ref}}$ is the reduced frequency and $St = \frac{kh}{\pi c}$ is the Strouhal number. The calculation of k uses the following values of reference velocity $U_{ref} = 1,4604$ m/s and a chord length of $c = 1$ m. All simulations run at $Re = 100,000$. The sinusoidal pitching movement is determined using this equation $\theta(t) = \theta_0 \sin(2\pi ft + \varphi)$. All simulated pitching motions use the values of $\varphi = 0^\circ$ and $\theta = 15^\circ$, where θ_0 is the pitching amplitude ($^\circ$), and φ is the phase difference between plunging motion and pitching motion ($^\circ$). The rotational axis is at 0.25-chord from the airfoil's leading edge. The tandem airfoil used in the simulation is shown in Figure 2 (a).

The effects of stagger on flapping airfoil propulsion were analyzed using NACA 0012 symmetrical airfoil with variations in the stagger of (X/c): 1, 1.5, 2, and 2.5. The effects of thickness on the flapping propulsion are studied using several symmetrical airfoils: NACA 0012, NACA 0015, NACA 0020, and NACA 0030. The study on the curvature of the airfoil is conducted using three variations of curvature (2%, 4%, and 6%) at a fixed position of 40% from the airfoil's leading edge: NACA 2430, NACA 4430, and NACA 6430. Fixed position of 40% means the maximum camber is located at 40% of the chord based on NACA's four-digit nomenclature. The direction of different kinds of forces is implemented in Figure 2 (b). Thrust force has the same direction as the airfoil (x-axis negative). Meanwhile, the drag force has the opposite direction to the thrust force (x-axis positive). And also, the lift force has a perpendicular direction to both thrust and drag force. Based on all the forces working on the airfoil, therefore the coefficient of performance and propulsive efficiency can be determined by Eq.(1) and Eq.(2), respectively.

$$CP = - [CL(t)\dot{h}(t) + CM(t)\dot{\theta}(t)]/U_{ref} \quad (1)$$

$$\eta_P = [-CD_{mean}/CP_{mean}] \times 100\% \quad (2)$$

In these equations, CP is power coefficient, CL is lift coefficient, CM is pitching moment coefficient, $\dot{h}(t)$ is plunging velocity, which is the first derivative of the plunging amplitude $h(t)$, $\dot{\theta}(t)$ is pitching velocity which is the first derivative of the pitching amplitude $\theta(t)$, CD_{mean} is time-averaged drag coefficient, $CT_{mean} = -CD_{mean}$ is time-averaged thrust coefficient and CP_{mean} is time-averaged power coefficient.

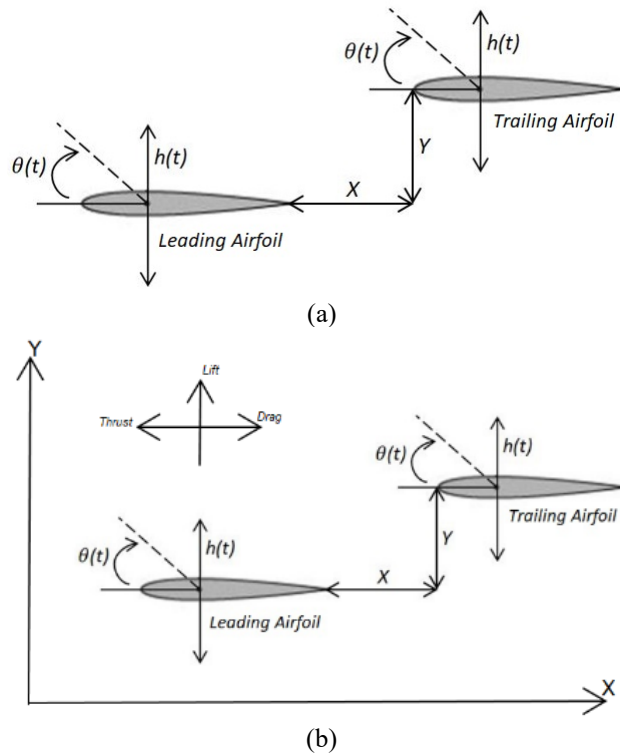


Figure 2 (a) Tandem airfoil combination design, and (b) direction of thrust force, lift force, and drag force tandem airfoil

3.0 RESULT AND DISCUSSION

3.1 Effects of Stagger

Figure 3(a) shows that the CD curves of the leading airfoil at each stagger are very similar to a single airfoil. The leading airfoil produces a high value of CD , as seen in Figure 3(a), which occurs at the time of $t/T = 0.155$. At that time, the lower surface of the leading airfoil has a green region, as seen in Figure 4. This color indicates that at the bottom of the leading airfoil, the airflow flows faster than at the leading airfoil's top. As a result, the air pressure at the top of the leading airfoil is higher than at the bottom of the leading airfoil. The cause is that at $t/T = 0.155$, the leading airfoil rotates in oscillation (pitching) and forms a pitching angle of -15° . The leading airfoil is in a nose-down position, thereby making airflow crash into the top of the leading edge. The airflow that hits the top of the airfoil's leading-edge flows through the upper and lower surfaces and creates a leading-edge vortex (LEV) at the bottom of the leading airfoil. This decreases the air pressure at the bottom of the leading airfoil and increases air pressure at the top of the leading airfoil.

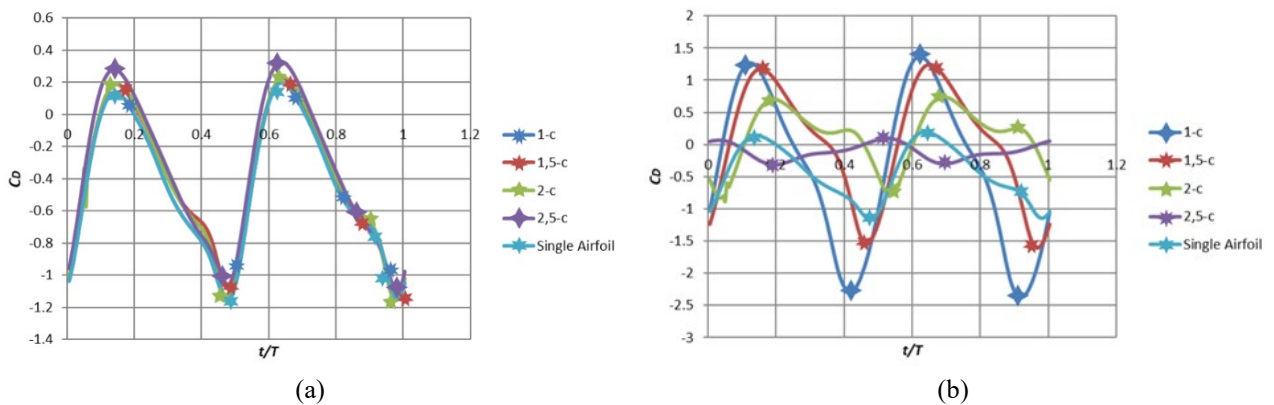


Figure 3. Time history of CD for tandem airfoil compared to CD of a single airfoil in (a) leading airfoil; (b) trailing airfoil conditions

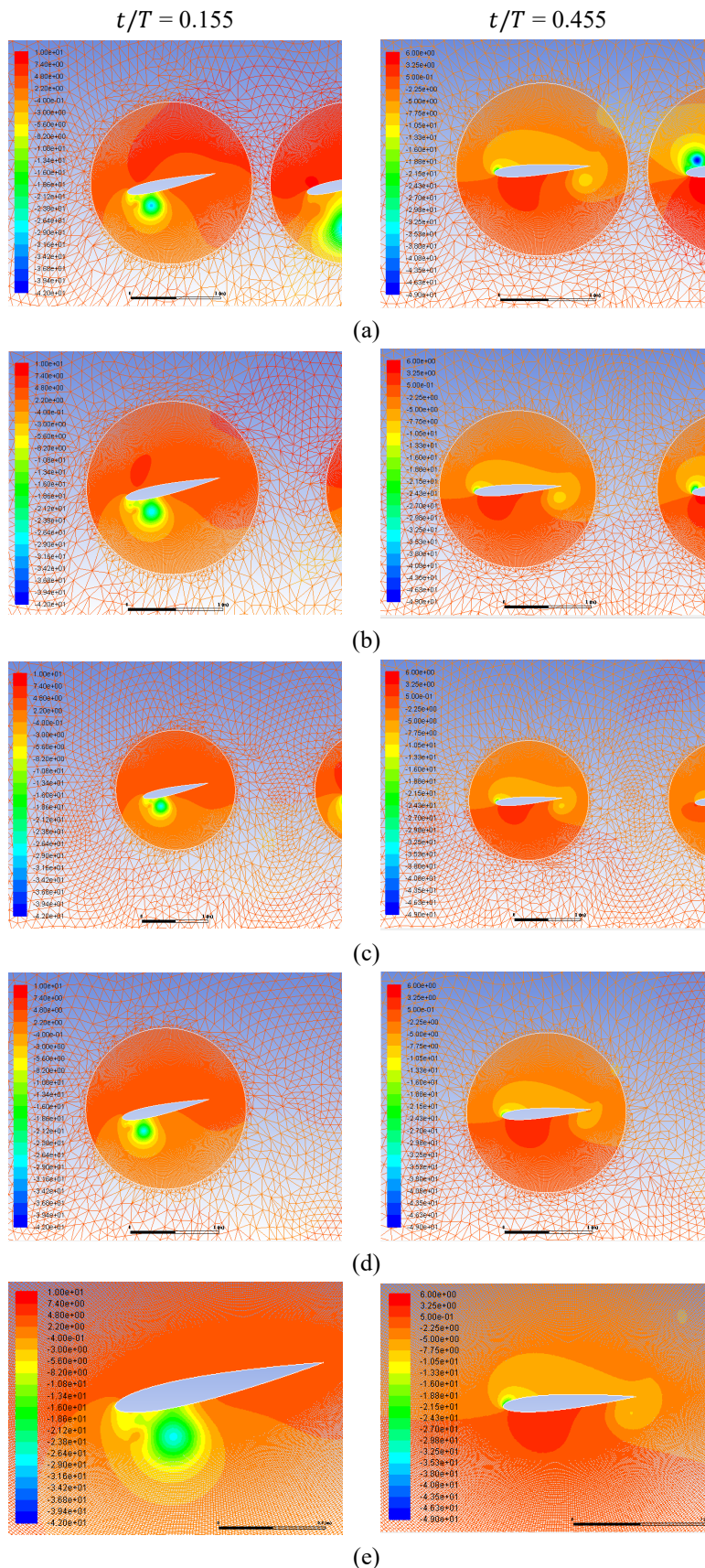


Figure 4. The pressure contours at $t/T = 0.155$ (left) and 0.455 (right) for the leading airfoil of (a) $X/c = 1$, (b) $X/c = 1.5$, (c) $X/c = 2$ and (d) $X/c = 2.5$, and (e) single airfoil

The opposite condition around the leading airfoil occurs at the time of $t/T = 0.455$. In this condition, the leading airfoil produces thrust CT ($=$ negative CD) values because the lower part of the leading airfoil experiences a higher air pressure than the upper part. As for the trailing airfoil shown in Figure 3(b), the tandem airfoil curve of each distance and the single airfoil produce different CD values throughout a flapping cycle. As shown by the graph in Figure 3(b), this

occurs at the time of $t/T = 0.205$ because, at that time, the trailing airfoils with X/c of 1, 1.5, and 2, as well as the single airfoil, produce CD , while the trailing airfoil with $X/c = 2.5$ produces CT . This occurs because the bottom of the trailing airfoil with a stagger of $X/c = 1, 1.5, 2$, and a single airfoil has a green circular region, which indicates that the LEV occurs at the bottom of the trailing airfoil. As a result of this phenomenon, the air pressure at the top of the trailing airfoil is higher than at the bottom. The air pressure at the top of the trailing airfoil becomes even higher because the airflow that has passed through the leading airfoil presses the top of the leading edge of the rear airfoil, as shown in Figure 5. Different conditions are experienced by the trailing airfoil at the distance of $X/c = 2.5$. Although the trailing airfoil is in a nose-down position like the other airfoils, the air pressure at the top of the trailing airfoil is lower than the air pressure under it.

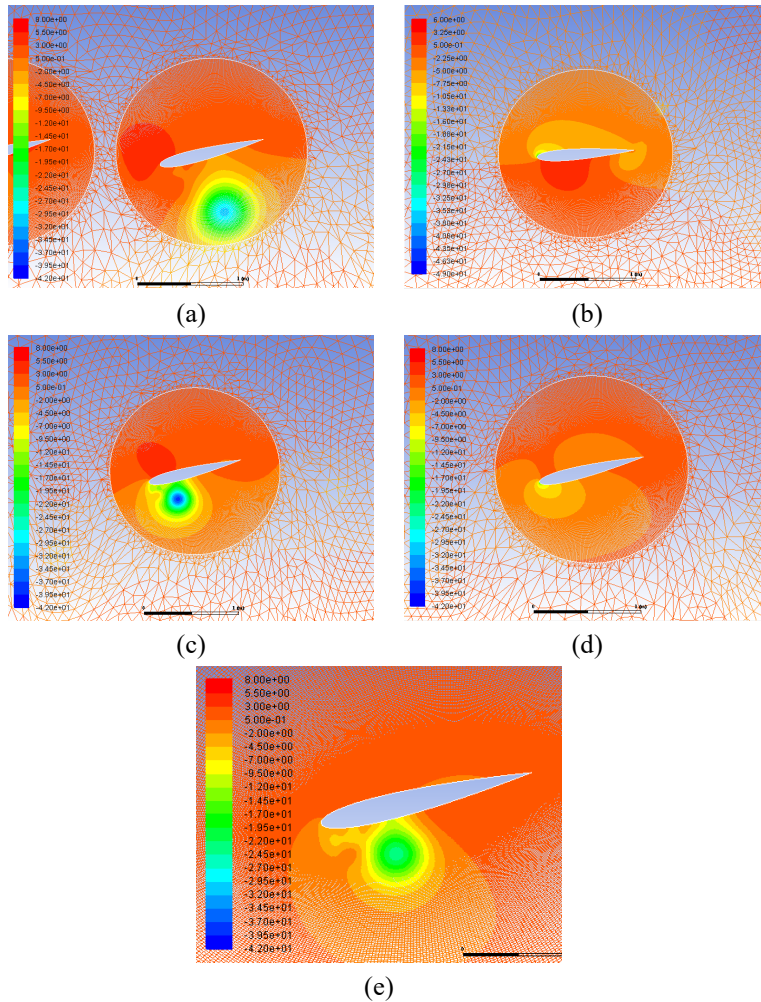


Figure 5. The pressure contours at $t/T = 0.205$ for trailing airfoil of (a) $X/c = 1$, (b) $X/c = 1.5$, (c) $X/c = 2$ and (d) $X/c = 2.5$, and (e) single airfoil

The time history of lift (CL) of the leading airfoil at each stagger is very similar to that of the single airfoil. As shown in Figure 6, the leading airfoil, trailing airfoil, and single airfoil at $t/T = 0.505$ produce the highest CL value, whereas the lowest CL value is produced at $t/T = 0.155$. The most interesting thing about the trailing airfoil occurs at the time of $t/T = 0$ because the CL value generated at that time varies for each tandem and single airfoil.

At the time of $t/T = 0.155$, all leading airfoils of tandem configuration and the single airfoil produce a negative lift coefficient. Negative values in CL indicate that a leading airfoil generates a downward force or downforce. This condition can be seen in Figure 4. As shown in Figure 4, the air pressure at the top of the airfoil is higher than at the bottom. In addition to producing high CD values, these conditions produce negative CL values. Both conditions are losses that must be avoided in flapping-wing flights. The airfoil condition at the time of $t/T = 0.505$ occurs because the air pressure at the bottom of the airfoil is higher than the pressure at the top of the airfoil, as shown in Figure 7. As a result, the airfoil generates a large lift force value. In addition to increasing lift force, this condition results in a decrease in drag force on airfoils.

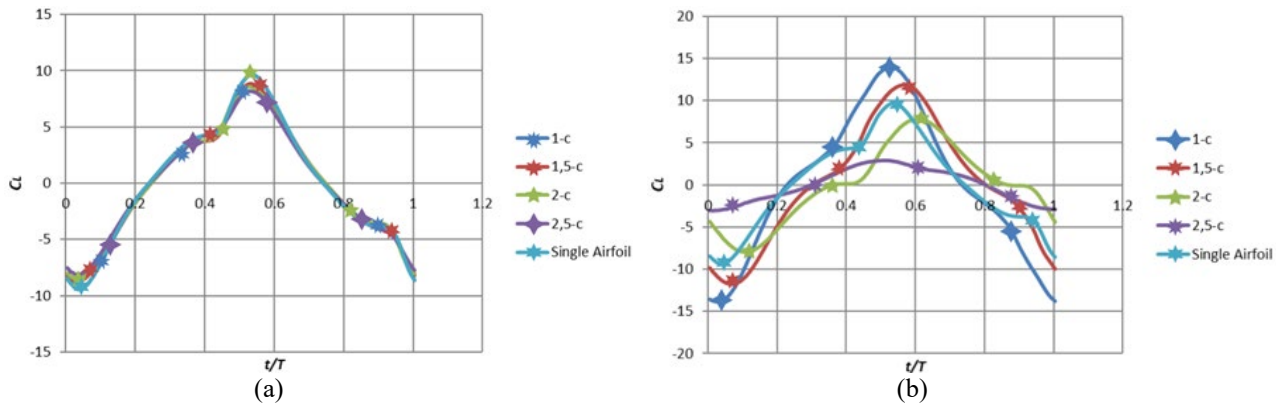


Figure 6. Time history of CL for tandem airfoil compared to CL of single airfoil in (a) leading airfoil and (b) trailing airfoil conditions

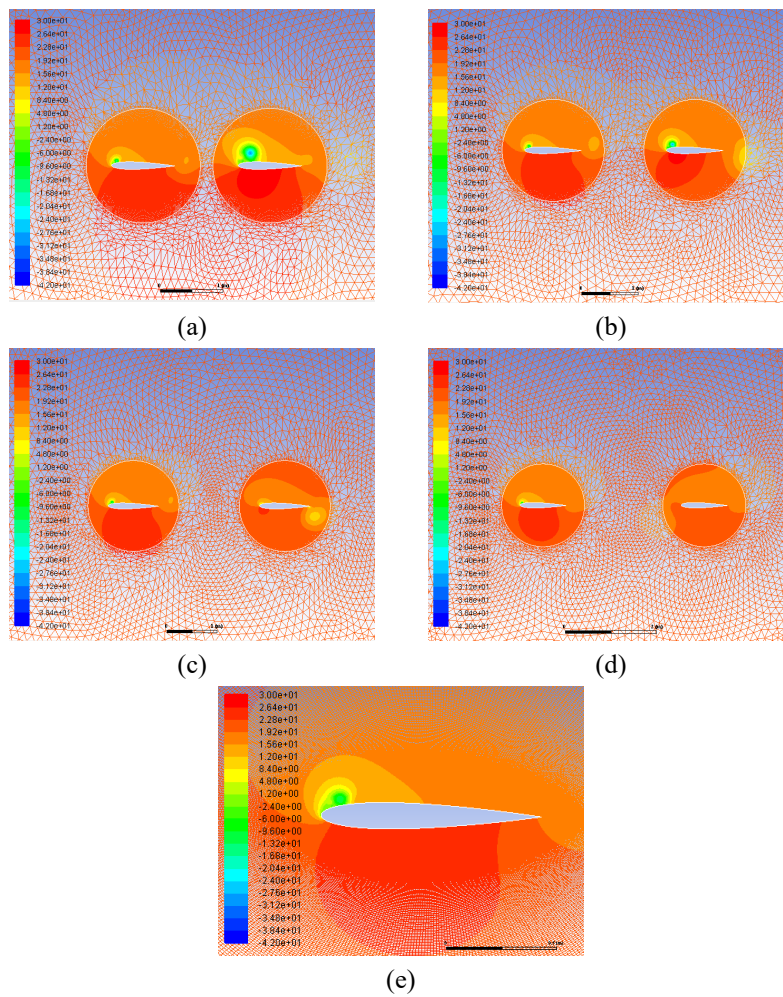


Figure 7. The pressure contours at $t/T = 0.505$ for tandem airfoil of (a) $X/c = 1$, (b) $X/c = 1.5$, (c) $X/c = 2$ and (d) $X/c = 2.5$, and (e) single airfoil

The high values of negative CL of the trailing airfoil at $t/T = 0$ are due to the LEVs that occur at the bottom surface, along with the proximity of the horizontal distance (stagger). This causes the pressure at the top of the trailing airfoil to increase and decrease the CL value, as shown in Figure 8. Thus, the closer the horizontal distance (stagger) is at $t/T = 0$, the lower the CL of the trailing airfoil will be.

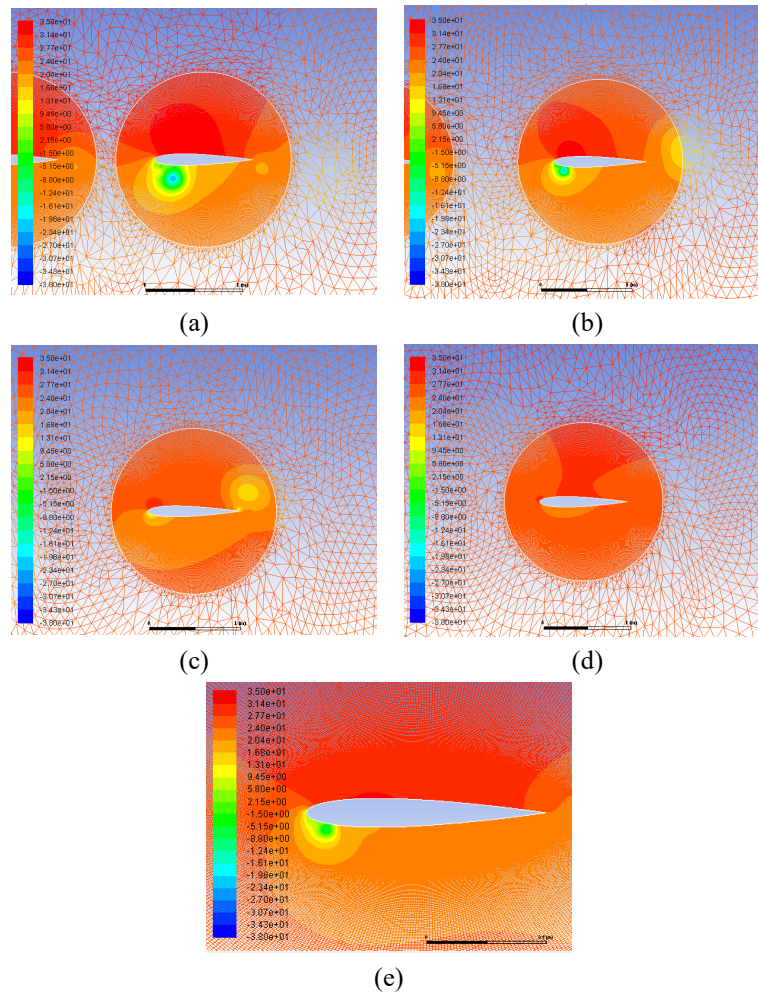


Figure 8. The pressure contours at $t/T = 0$ for trailing airfoil of (a) $X/c = 1$, (b) $X/c = 1.5$, (c) $X/c = 2$ and (d) $X/c = 2.5$, and (e) single airfoil

In Figure 9, the CT_{mean} , CL_{mean} , and CP_{mean} of one single airfoil are higher than tandem airfoils. CT_{mean} of the trailing airfoil decreases from the distance of $X/c = 1$ to $X/c = 2$ but rises again at $X/c = 2.5$. However, for the leading airfoil, CT_{mean} decreases with the stagger. The CL_{mean} of the leading and the trailing airfoil produce the same pattern, which decreases from the distance of $X/c = 1$ to $X/c = 1.5$, but the value increases back at the distance of $X/c = 2$ and decreases again at the distance of $X/c = 2.5$. CP_{mean} of the leading and the trailing airfoil decreases with the stagger. As seen in Figures 9(a) and 9(b), CT_{mean} and CL_{mean} of the leading airfoil at $X/c = 1$ are the highest, while, as seen in Figure 9(c), the CP_{mean} of the trailing airfoil at $X/c = 1$ and 1.5 are the highest.

The propulsive efficiency of the tandem airfoil is lower than the total efficiency of two single airfoils, as shown in Figure 10. In addition, the lowest value of propulsive efficiency of the tandem airfoil occurs at the stagger of $X/c = 2$, while the highest value of the propulsive efficiency of the tandem airfoil occurs at the stagger of $X/c = 2.5$. This pattern of propulsive efficiency continues to drop as the stagger (X/c) increases from 1 to 2 before rising again at $X/c = 2.5$ is the opposite of the research outcomes of Tuncer and Platzer [9]. However, it is important to note that the simulation settings of the two studies are different. This study is conducted at $Re = 1 \times 10^5$, $k = 2$, $h/c = 0.5$ and a vertical distance (Y_{shift}) of $0c$, while the study of Tuncer and Platzer [9] was done at $Re = 3 \times 10^6$, $k = 0.75$, $h/c = 0.2$ and a vertical distance (Y_{shift}) of $1c$. The combination of Reynolds number, plunging amplitude, reduced frequency and vertical distance between airfoils results in a different flow phenomena, which is reflected by the different results observed in this paper and previous work [9].

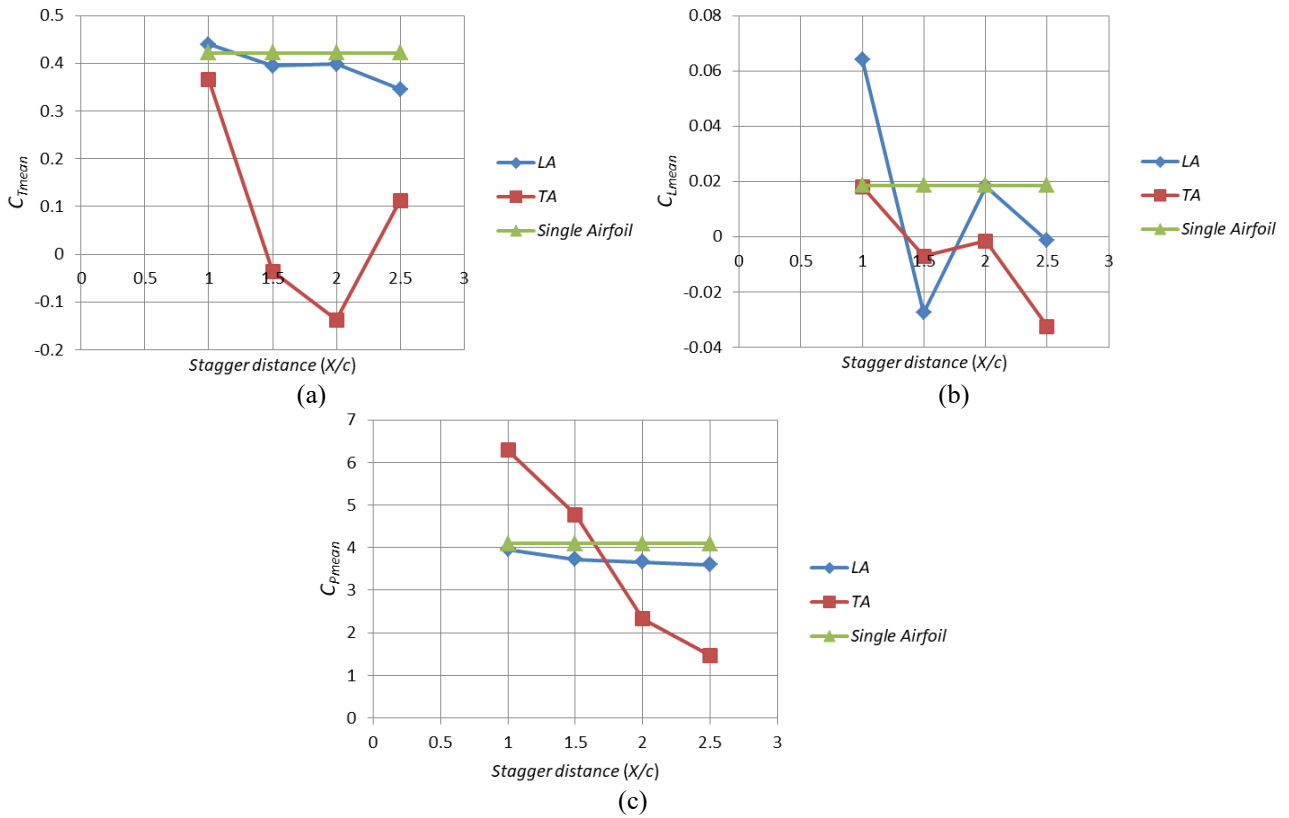


Figure 9. (a) C_{Tmean} , (b) C_{Lmean} and (c) C_{Pmean} of tandem airfoil compared to single airfoil

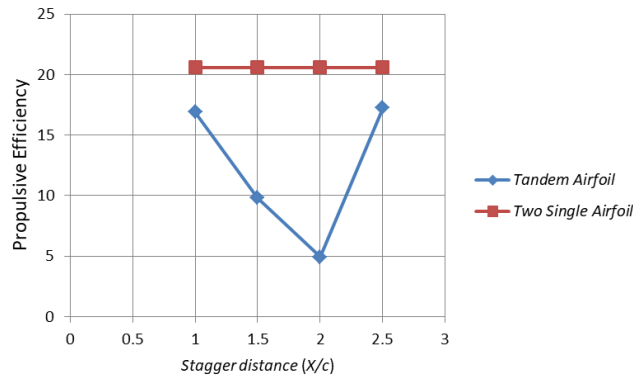


Figure 10. Propulsive efficiency of tandem airfoil compared to two single airfoils

3.2 Effect of Thickness

The simulation of thickness variation uses the stagger of $X/c = 2.5$ because the highest total efficiency of the tandem airfoil propulsion is produced at that distance. From Figure 11, the CD curve of the tandem airfoil for each thickness in the same cycle varies. The leading airfoil condition produces a CD value, as shown by the graph in Figure 11(a), which occurs at the time of $t/T = 0.205$. This is due to the LEVs phenomenon at the bottom of the leading airfoil, which causes low air pressure at the bottom of the leading airfoil. The top leading airfoil experiences high air pressure, resulting in a drag force for leading airfoils. The thicker the leading airfoil is, the smaller the size of LEVs will be. This affects the leading airfoil CD value produced, as seen in Figure 12.

At the time of $t/T = 0.405$, the leading airfoil produces CT values. The high air pressure occurs at the bottom of all leading airfoils, resulting in a force driving the leading airfoil forward, and at the same time, the trailing airfoil produces a CD value. As a result of the air pressure at the front of the trailing airfoil, the trailing airfoil experiences a drag force at $t/T = 0.405$. The difference in thickness leads to a significant difference in the air pressure at the bottom of the airfoil.

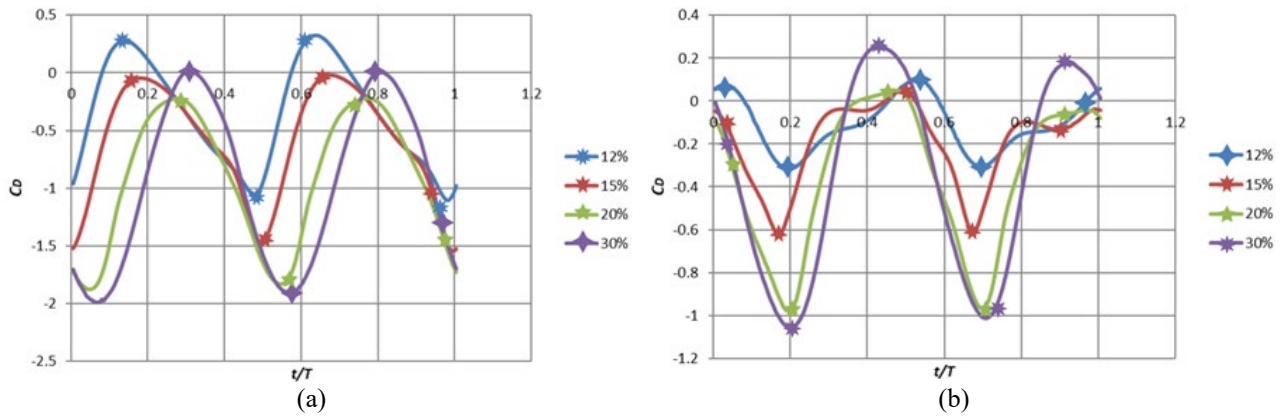


Figure 11. Time history of C_D for tandem airfoil in (a) leading airfoil; (b) trailing airfoil conditions

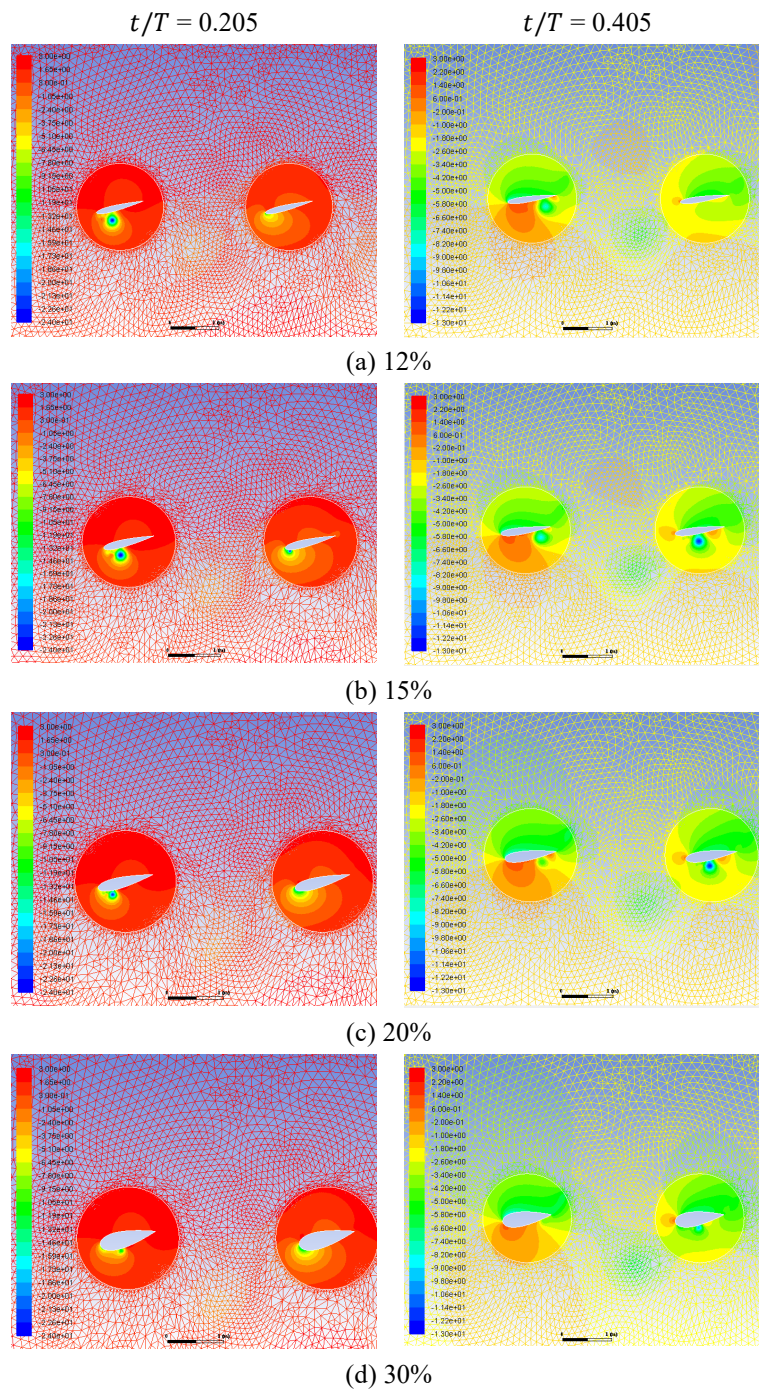


Figure 12. The pressure contours at $t/T = 0.205$ and 0.405 for different tandem airfoil thicknesses

As for the CL curve, the tandem airfoil in each thickness tested is generally the same. As shown by the graph in Figure 13(a), the leading airfoil produces the highest CL value at the time of $t/T = 0.505$. This is caused by the air pressure at the bottom of the leading airfoil, which is higher than the top, as seen in Figure 14. The difference in thickness results in a difference in the value of CL of the leading airfoil. The air pressure that occurs on the leading airfoil with a thickness of 12% is larger than that of 30%. It is proved by the value of CL at that time of $t/T = 0.505$ value of CL on leading airfoil with 12% thickness is 7.699, while the value of CL on the leading airfoil with 30% thickness is 7.306.

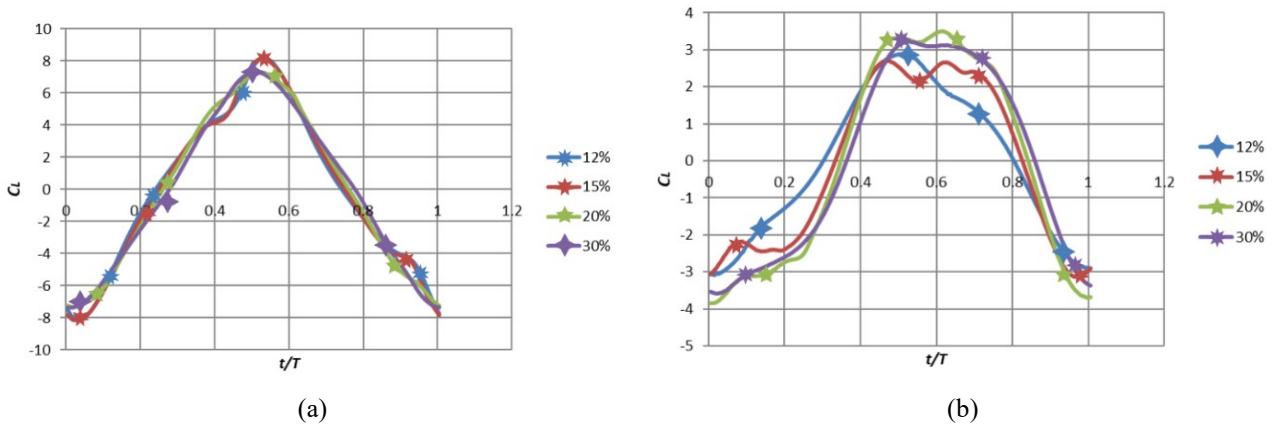


Figure 13. Time history for CL tandem airfoil in (a) leading airfoil; (b) trailing airfoil conditions

As seen in Figure 13(b), the trailing airfoil produces a downforce at $t/T = 0.205$. The reason is that the air pressure at the top of the trailing airfoil is higher at the bottom, which at that time causes the downward force on all trailing airfoils, as seen in Figure 12. Meanwhile, the opposite condition occurs at the time of $t/T = 0.505$ because the air pressure at the bottom of the trailing airfoil at that time is higher than at the top of the trailing airfoil (shown in Figure 14).

In Figure 15, the single airfoil values still dominate CT_{mean} , CL_{mean} , and CP_{mean} values. The greater the thickness of the airfoil, the higher value of CT_{mean} is. The CT_{mean} of the leading airfoil value is higher than the CT_{mean} of the trailing airfoil value. The CL_{mean} of the single airfoil with a thickness of 12% and 15% produces the highest value, but a thickness of 20% and 30% yields the lowest CL_{mean} value. The CT_{mean} of the leading airfoil value is higher than the trailing airfoil. The single airfoil CL_{mean} with 12% and 15% thickness yields the highest value, but the thickness of 20% and 30% produces the lowest CL_{mean} values. For the CP_{mean} single airfoil produces a higher value than leading or trailing airfoil. The highest value of CP_{mean} leading airfoil is 15% thickness, with the value of CP_{mean} being 3.664. While the highest value of CP_{mean} is 20% thickness, the value of CP_{mean} is 1.762.

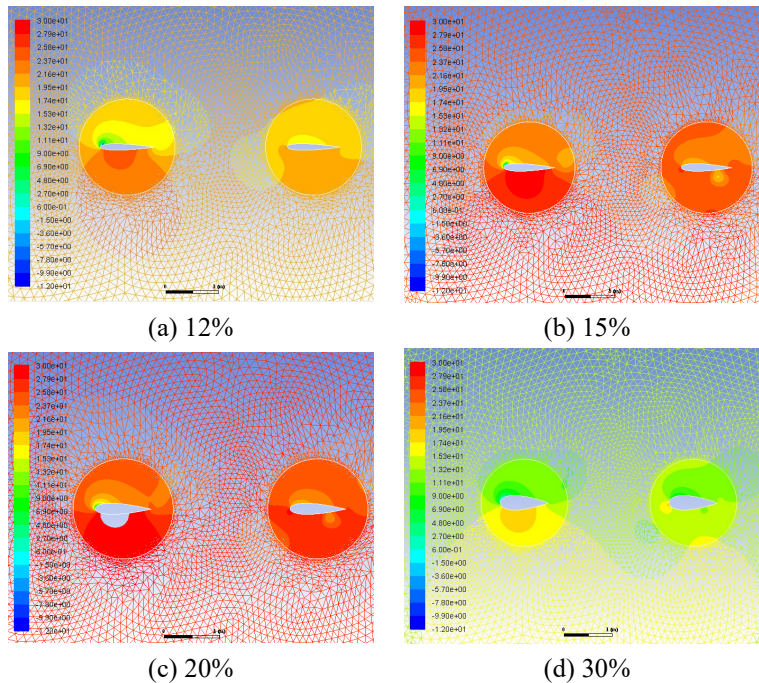


Figure 14. The pressure contours at $t/T = 0.505$ at different tandem airfoil thicknesses

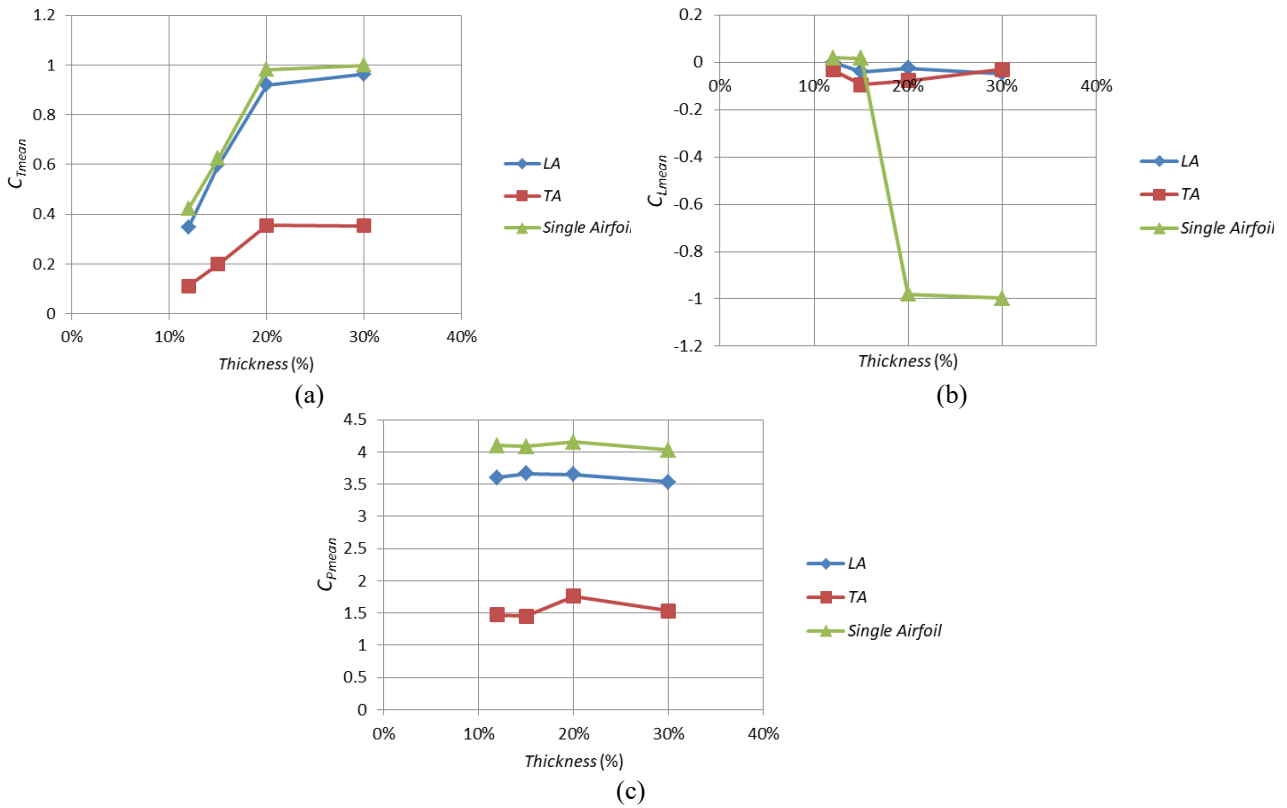


Figure 15. (a) C_{Tmean} , (b) C_{Lmean} and (c) C_{Pmean} of tandem airfoil compared to a single airfoil

Figure 16 shows that the increase in the thickness of the airfoil raises the value of propulsive efficiency. The value of propulsive efficiency of a tandem airfoil is higher than the total efficiency of two single airfoils. Compared with the efficiency of two single airfoil propulsion, the difference in the efficiency of the tandem airfoil is in the range of 2% - 4%.

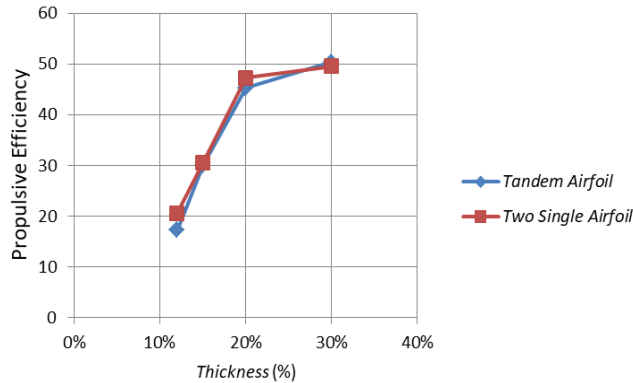


Figure 16. Propulsive efficiency of tandem airfoil compared to two single airfoils

3.3 Effect of Curvature

The simulations of curvature variations use the stagger of $X/c = 2.5$ and the thickness of 30% because the highest efficiency value is produced at this combination of distance and thickness. Figure 17 shows that the CD curve of the tandem airfoil in each curvature is very similar. The leading airfoil produces the highest CD value at the time of $t/T = 0.855$. The increase in curvature results in the rise in CD . This is due to the pressure on the bottom surface becoming higher as the curvature increases (shown in Figure 18). Meanwhile, the opposite condition occurs at $t/T = 0.505$, with the leading airfoil producing thrust (CT). The trailing airfoil produces the highest CD value at the time of $t/T = 0.405$, as seen in Figure 17. Like the leading airfoil, the curvature affects the CD values of the trailing airfoil. Meanwhile, the opposite condition occurs at the time of $t/T = 0.705$, and an increase in curvature results in a smaller thrust (CT). In Figure 18, trailing airfoils produce positive CD values at $t/T = 0.405$ because LEVs are formed at the bottom of all trailing airfoils. The trailing airfoil with 0% curvature has $CD = 0.237$, while the trailing airfoil with 6% curvature has a CD of 0.371.

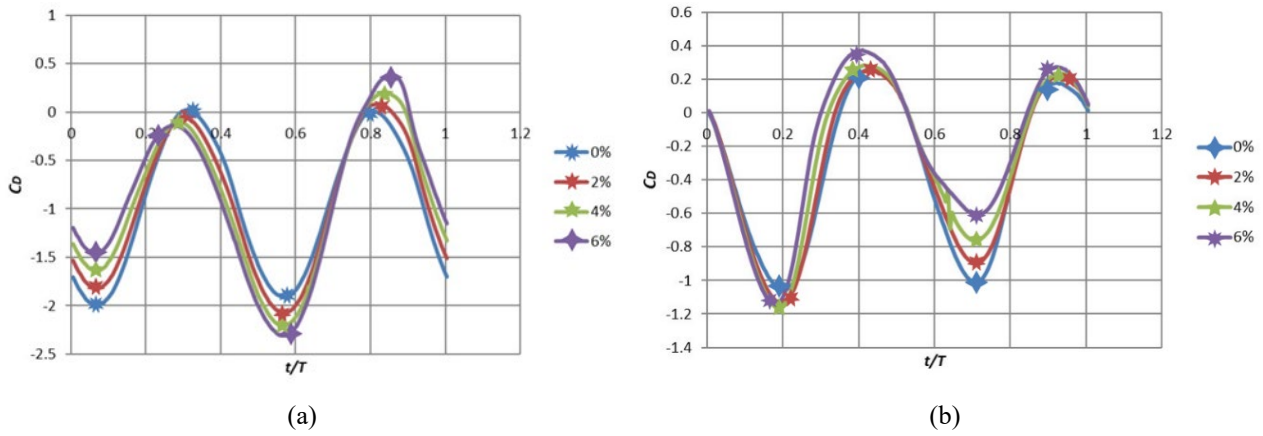


Figure 17. Time history of CD for tandem airfoil in (a) leading airfoil and (b) trailing airfoil conditions

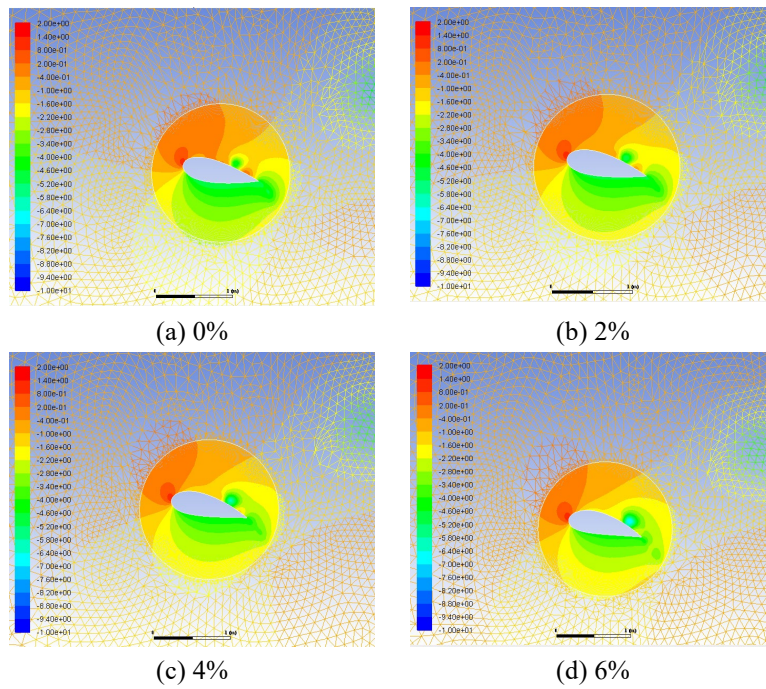


Figure 18. The pressure contours at $t/T = 0.805$ at different tandem airfoil curvatures

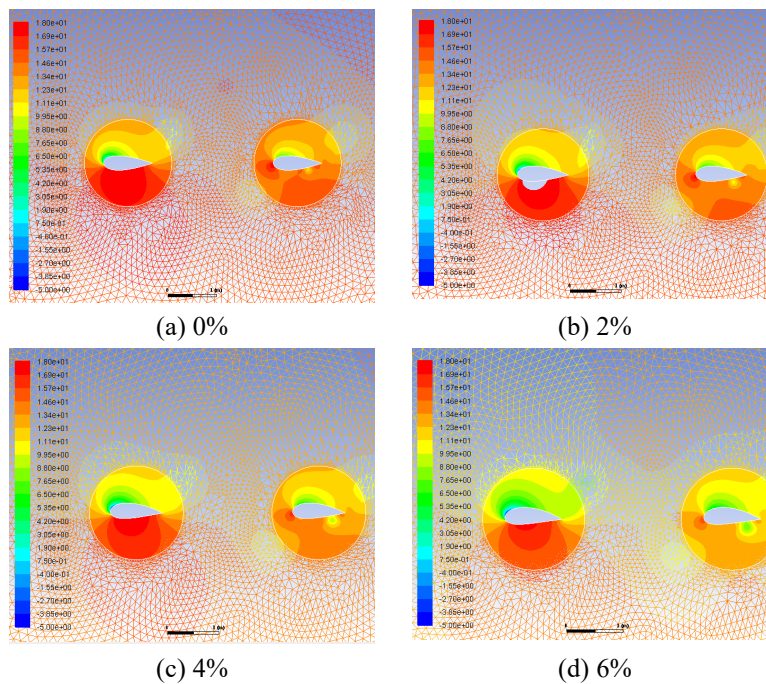


Figure 19. The pressure contours at $t/T = 0.405$ with different curvatures

The tandem airfoil produces the highest CL value at $t/T = 0.505$. Meanwhile, the opposite condition occurs at the time of $t/T = 0.205$, as seen in Figure 20. At the time of $t/T = 0.205$, air pressure on leading airfoils produces downforce (Figure 21). The rise in the curvature of leading airfoils results in a higher CL with less downforce being generated. At this time, the leading airfoil with 0% curvature has $CL = -2.346$, while the 6% has a CL value of 1.269.

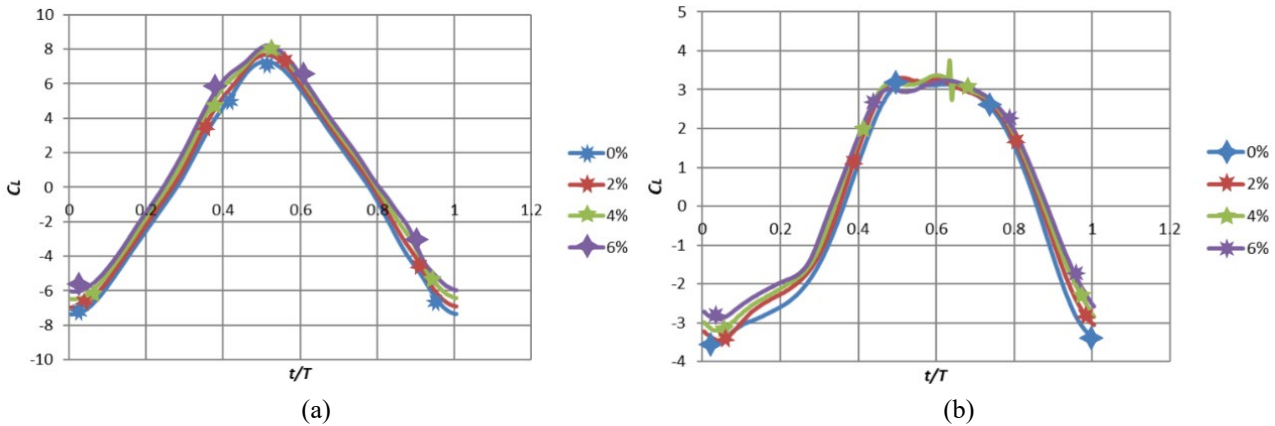


Figure 20. Time history for CL tandem airfoil in (a) leading airfoil and (b) trailing airfoil conditions

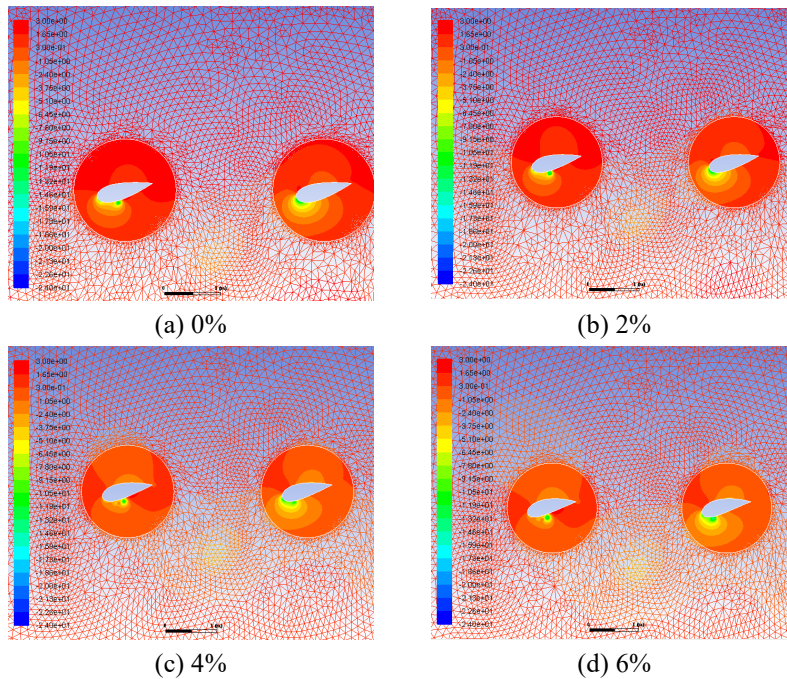
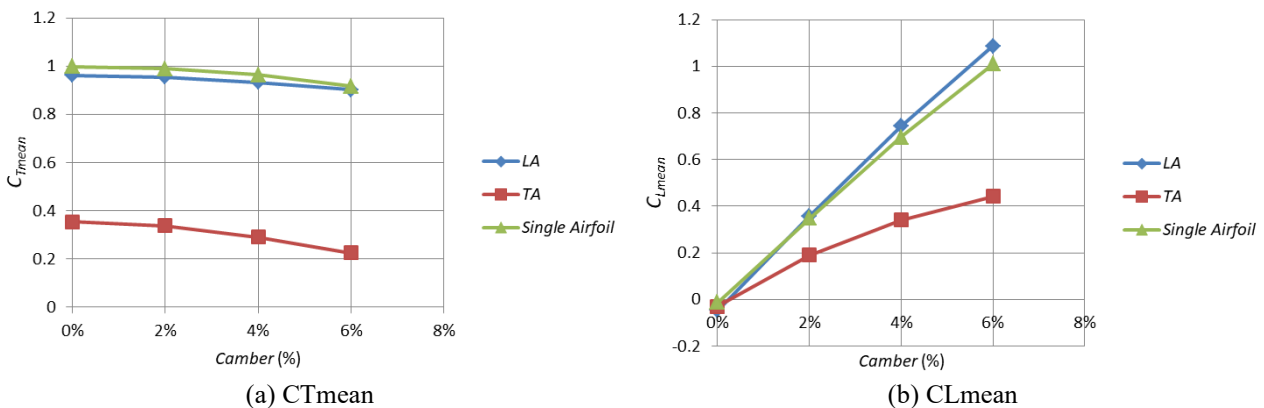


Figure 21. The pressure contours at $t/T = 0.205$ for tandem airfoil at different curvatures

Similar to previous findings, the single value is greater than the leading airfoil or trailing airfoil except for the CL_{mean} , where the CL_{mean} of the leading airfoil is greater. As for CT_{mean} and CP_{mean} , the value decreases as the curvature of the airfoil increases. However, CL_{mean} rises with the curvature, as seen in Figure 22. Figure 23 shows that the greater the airfoil curvature reduces the propulsive efficiency of an airfoil, and the greatest reduction happens in the tandem airfoil.



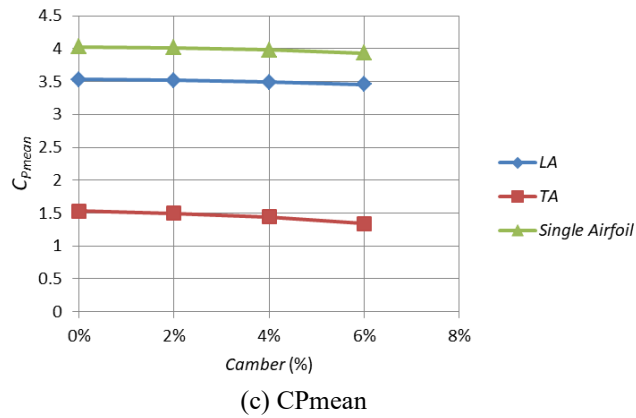


Figure 22. CTmean, CLmean and CPmean of tandem airfoil compared to a single airfoil

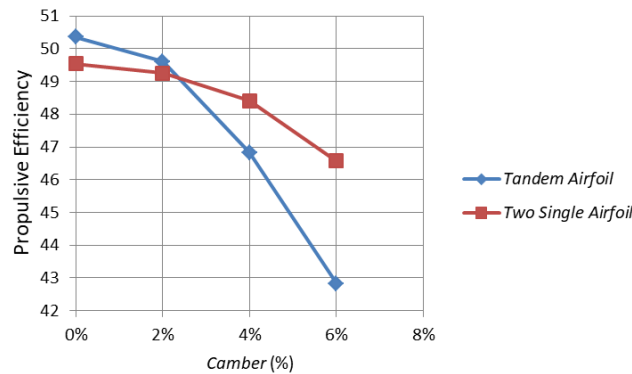


Figure 23. Propulsive efficiency of tandem airfoil compared to two single airfoils (NACA 0030)

4.0 CONCLUSIONS

The simulations were done with a four-digit NACA airfoil at Reynolds number 100,000, with non-dimensional numbers $h = 0.5$ and $k = 2$ ($St = 0.31$). It can be concluded that the stagger of $2.5c$ is the most optimum distance because it produces the highest total propulsive efficiency among the other stagger distance in this study. For thickness variation, it can be concluded that airfoils with 30% thickness have the highest total propulsive efficiency among the other thickness variations in this study. As for the curvature variations, the propulsive efficiency decreases with the increasing curvature. This decrease in the propulsive efficiency of a tandem airfoil is more significant than that of two single airfoils. The results of this study provide insight into the aerodynamics of flapping tandem airfoils. This is valuable insight because most published works on the aerodynamics of flapping airfoils/wings focus on a single airfoil. The outcomes of this study regarding the most optimum stagger, airfoil thickness and curvature might also benefit engineers and designers of water/wind turbines and micro air vehicles.

5.0 ACKNOWLEDGEMENT

This research was funded by Kementerian Pendidikan, Kebudayaan, Riset, dan Teknologi under the Penelitian Dasar Kompetitif Nasional research scheme number NKB-994/UN2.RST/HKP.05.00/2022.

6.0 REFERENCES

- [1] W. Shyy, H. Aono, C. Kang, and H. Liu, "An introduction to flapping wing aerodynamics," United Kingdom: Cambridge University Press, 2013.
- [2] H. Djojodihardjo and A. S. S. Ramli, "Modeling studies of bi- and quad-wing flapping ornithopter kinematics and aerodynamics," *International Journal of Automotive and Mechanical Engineering*, vol. 9, pp. 1669–1684, 2022.
- [3] D. Bie and D. Li, "Numerical analysis of the wing-wake interaction of tandem flapping wings in forward flight," *Aerospace Science and Technology*, vol. 121, p. 107389, 2022.
- [4] C. Liu, P. Li, F. Song, E. J. Stamhuis, and J. Sun, "Design optimization and wind tunnel investigation of a flapping system based on the flapping wing trajectories of a beetle's hindwings," *Computers in Biology and Medicine*, vol. 140, p. 105085, 2022.
- [5] Z. Wang, Z. Kan, H. Li, D. Li, S. Zhao, and Z. Tu, "Parametric study on aerodynamic performance of a flapping wing rotor MAV capable of sustained flight," *Aerospace*, vol. 9, no. 10, p.551, 2022.
- [6] D. A. Olejnik *et al.*, "An experimental study of wind resistance and power consumption in MAVs with a low-speed multi-fan wind system," In 2022 International Conference on Robotics and Automation (ICRA), May 2022, pp. 2989–2994.
- [7] A. Joda, A. O. Mohammed, and E. Tolouei, "A parametric study on the propulsion performance of MAVs flapping foils," In 2022 Advances in Science and Engineering Technology International Conferences (ASET), Feb. 2022, pp. 1–6.
- [8] M. M. Koochesfahani, "Vortical patterns in the wake of an oscillating airfoil," *AIAA Journal*, vol. 27, pp. 1200–1205, 1987.

- [9] I. H. Tuncer and M. F. Platzer, "Thrust generation due to airfoil flapping," *AIAA Journal*, vol. 34, no. 2, pp. 324–331, 1996.
- [10] K. D. Jones, T. C. Lund, and M. F. Platzer, "Experimental and computational investigation of flapping wing propulsion," *Fixed and Flapping Wing Aerodynamics for Micro Air Vehicle Application*, vol. 195, pp. 307–336, 2001.
- [11] J. Reuster and J. Baeder, "Dynamic stall from pitching and plunging airfoil motions," in *1st Flow Control Conference*, St. Louis, Missouri, 2002, p. 3272.
- [12] J.-S. Lee, J.-H. Kim, and C. Kim, "Numerical study on the unsteady-force-generation mechanism of insect flapping motion," *AIAA Journal*, vol. 46, no. 7, pp. 1835–1848, 2008.
- [13] D. Rival and C. Tropea, "Characteristics of pitching and plunging airfoils under dynamic-stall conditions," *Journal of Aircraft*, vol. 47, no. 1, pp. 80–86, 2010.
- [14] P. Wu and P. Ifju, "Experimental methodology for flapping wing structure optimization in hovering flight of micro air vehicles," in *51st AIAA/ASME/ASCE/AHS/ASC Structures, Structural Dynamics, and Materials Conference*, 2010, p. 2709.
- [15] H. Hu, W. Ren, H. Liu, and J. Wu, "An experimental investigation on the asymmetric wake of an oscillating airfoil," in *51st AIAA Aerospace Sciences Meeting Including the New Horizons Forum and Aerospace Exposition*, 2013, p. 794.
- [16] H. W. Hoeijmakers and J. Mulder, "Computational and experimental investigation into flapping wing propulsion," in *54th AIAA Aerospace Sciences Meeting*, 2016, p. 0802.
- [17] A. Brentjes and H. W. Hoeijmakers, "Experimental investigation into wake flapping wing robotic bird," in *35th AIAA Applied Aerodynamics Conference*, 2017, p. 3409.
- [18] M. A. Ashraf, J. Young, and J. C. S. Lai, "Reynolds number, thickness and camber effects on flapping airfoil propulsion," *Journal of Fluids and Structures*, vol. 27, no. 2, pp. 145–160, 2011.
- [19] M. Yu, Z. J. Wang, and H. Hu, "High fidelity numerical simulation of airfoil thickness and kinematics effects on flapping airfoil propulsion," *Journal of Fluids and Structures*, vol. 42, pp. 166–186, 2013.
- [20] W. Null and S. Shkarayev, "Effect of camber on the aerodynamics of adaptive-wing micro air vehicles," *Journal of Aircraft*, vol. 42, no. 6, pp. 1537–1542, 2005.
- [21] D. Ma, Y. Zhao, Y. Qiao, and G. Li, "Effects of relative thickness on aerodynamic characteristics of airfoil at a low Reynolds number," *Chinese Journal of Aeronautics*, vol. 28, no. 4, pp. 1003–1015, 2015.
- [22] I. Tuncer and M. Platzer, "A computational study of flow separation characteristics and wake profiles behind a flapping airfoil," in *37th Aerospace Sciences Meeting and Exhibit*, 1999, p. 648.
- [23] T. Broering, Y. Lian, and W. Henshaw, "Numerical study of two flapping airfoils in tandem configuration," in *48th AIAA aerospace sciences meeting including the new horizons forum and aerospace exposition*, 2010, p. 865.
- [24] T. Broering and Y. Lian, "The effect of wing spacing on tandem wing aerodynamics," in *28th AIAA Applied Aerodynamics Conference*, 2010, p. 4385.
- [25] K. B. Lim and W. B. Tay, "Numerical analysis of the S1020 airfoils in tandem under different flapping configurations," *Acta Mechanica Sinica*, vol. 26, no. 2, pp. 191–207, 2010.
- [26] X. Zhang, K. B. Lua, T. T. Lim, and K. S. Yeo, "Experimental study of two-dimensional flapping wings in tandem configuration," in *43rd AIAA Fluid Dynamics Conference*, 2013, p. 2468.
- [27] A. S. Bin Azry Seet, H. Tang, and S. Yu Ching Man, "Experimental study of flow over two oscillatory pitching airfoils in tandem configuration," in *31st AIAA Applied Aerodynamics Conference*, 2013, p. 2817.
- [28] Y.-H. Lai, S.-K. Chang, B. Lan, K.-L. Hsu, and J.-T. Yang, "Optimal thrust efficiency for a tandem wing in forward flight using varied hindwing kinematics of a damselfly," *Physics of Fluids*, vol. 34, no. 6, p. 061909, 2022.
- [29] N. Hosseini, M. Tadjfar, and A. Abba, "Configuration optimization of two tandem airfoils at low Reynolds numbers," *Applied Mathematical Modelling*, vol. 102, pp. 828–846, 2022.
- [30] Z. Chen, X. Li, and L. Chen, "Enhanced performance of tandem plunging airfoils with an asymmetric pitching motion," *Physics of Fluids*, vol. 34, no. 1, p. 011910, 2022.
- [31] G. Wang, B.F. Ng, Z.W. Teo, K.B. Lua, and Y. Bao, "Performance augmentation mechanism of tandem flapping foils with stroke time-asymmetry," *Aerospace Science and Technology*, vol. 117, p. 106939, 2021.
- [32] J. Alba-Maestre, Koen Prud'homme van Reine, T. Sinnige, and S. G. P. Castro, "Preliminary propulsion and power system design of a tandem-wing long-range eVTOL aircraft," *Applied Sciences*, vol. 11, no. 23, p. 11083, 2021.
- [33] Z. Liu, B. Hyun, M. Kim, and J. Jin, "Experimental and numerical study for hydrodynamic characteristics of an oscillating hydrofoil," *Journal of Hydrodynamics, Ser. B*, vol. 20, no. 3, pp. 280–287, 2008.
- [34] J. Young, M.A. Ashraf, J.C.S. Lai, and M.F. Platzer, "Numerical simulation of fully passive flapping foil power generation," *AIAA Journal*, vol. 51, no. 11, pp. 2727–2739, Nov. 2013.
- [35] J. Xu, H. Sun, and S. Tan, "Wake vortex interaction effects on energy extraction performance of tandem oscillating hydrofoils," *Journal of Mechanical Science and Technology*, vol. 30, no. 9, pp. 4227–4237, 2016.
- [36] S. N. Ashwindran, A. A. Aziz, and A. N. Oumer, "Unsteady computational study of novel biologically inspired offshore vertical axis wind turbine at different tip speed ratios: A two-dimensional study," *International Journal of Automotive and Mechanical Engineering*, vol. 16, no. 2, pp. 6753–6772, 2019.
- [37] C. Read and H. Viswanathan, "An aerodynamic assessment of vehicle-side wall interaction using numerical simulations," *International Journal of Automotive and Mechanical Engineering*, vol. 17, no. 1, pp. 7587–7598, 2020.
- [38] S. Mohanty and R. Arora, "CFD analysis of a shell and tube heat exchanger with single segmental baffles," *International Journal of Automotive and Mechanical Engineering*, vol. 17, no. 2, pp. 7890–7901, 2020.